









Load-settlement and skin friction behaviour of piles in dry sand: experimental and numerical study

VEDPRAKASH C MARALAPALLE^{1,*}, MAHEBOBSAB B NADAF²,
SUSHOVAN DUTTA³, AIJAZ AHMAD ZENDE⁴, S SANGITA MISHRA¹
and SHRIKANT CHARHATE¹

¹Department of Civil Engineering, Amity School of Engineering and Technology, Amity University Maharashtra, Mumbai – Pune Expressway, Bhatan, Post – Somathne, Panvel, Mumbai, Maharashtra 410206, India

²Department of Civil Engineering, Thakur College of Engineering and Technology, Mumbai, Maharashtra 400101, India

³Department of Civil Engineering, National Institute of Technology Durgapur, Durgapur, West Bengal 713209, India

⁴Department of Civil Engineering, BLDEA's Vachana Pitamaha Dr. P.G Halakatti College of Engineering and Technology, Vijayapur, Karnataka 586103, India

e-mail: vcmaralapalle@mum.amity.edu; maheboobnadaf380@gmail.com; sushovan.dutta@ce.nitdgp.ac.in; aijaz.52964@gmail.com; ssmishra@mum.amity.edu; scharhate@mum.amity.edu

MS received 19 July 2023; revised 23 September 2023; accepted 18 October 2023

Abstract. The objective of the study was to evaluate the load-settlement behaviour of piles, both with and without the inclusion of a sponge material at the pile base to minimize tip resistance and enhance skin friction. Laboratory experiments were conducted to examine the response of pile models subjected to axial loads in dry sand. Physical scaling principles were meticulously applied to determine model pile dimensions and tank size, which were dependent on the material properties of the model. The modelled pile, fabricated using aluminium, had an external diameter of 60 mm. The investigation encompassed pile length-to-diameter ratios of 4 and 6. Axial loads and skin friction were quantified using strain gauge measurements. Furthermore, numerical modelling of the experimental tests was conducted using PLAXIS 3D, where the sand was represented using a hardening soil model and the pile was modelled elastically. Triaxial tests were performed on sand samples to characterize soil properties, and laboratory tests were executed to ascertain pile parameters. To account for soil-pile interaction, interface elements were introduced between the soil and pile. Multiple parametric studies were undertaken by varying pile configurations, and subsequent numerical results were systematically compared with the experimental findings. Numerical models correctly represented pile's behaviour under various loading circumstances. Less than $\pm 5\%$ of displacement difference was detected between experimental and numerical findings, demonstrating acceptable agreement between the two methods.

Keywords. Skin friction; pile foundation; FEM; displacement; axial load.

1. Introduction

Pile foundations have become more popular in recent years for reducing average and unequal settlement of building foundation. Bridges, high rise structures that may be subjected to axial, lateral, and overturning loads [1, 2]. In situations where the upper layer of soil is not able to provide sufficient support for a structure, in order to distribute the load to a deeper level, a pile foundation is commonly utilized. The combined action of mobilized skin resistance and

base resistance is employed to resist the applied load [3–5]. Open-ended and closed-ended piles were driven into sand and conducted field pile load testing to assess the impact of the soil plug on their static and cyclic actions. The open-ended pile had a lower cumulative hammer blow count and lower limit unit shaft and base resistances against to the closed-ended pile [6]. To examine the behavior of driven and jacked H-piles, a thorough field investigation was carried out. In leftover soils that are similar to silty sands, instrumented piles were installed. The findings indicated that driven piles frequently exhibited lesser base resistance but stiffer and greater shaft resistance than jacked piles [7].

*For correspondence

One of the most established and commonly used piling methods is the cast-in-situ pile, can be used in a variety of surface, comprising soil and rock [8–10]. Nevertheless, it is essential to ensure that the drilled hole is properly cleaned to eliminate any sediment or drilling debris at the tip of the pile [11, 12]. In cases where weak sediments are present at the pile base, settling may occur before reaching the desired end resistance. Researchers have identified the presence of surrounding and bottom debris as a contributing factor to pile bearing problems [13–15]. Baoyun *et al* [16] studied the performance of model pile foundations subjected to static loads in dry sand was examined. In this investigation, the base of the modelled pile was kept on the sand layer, thus the pile was treated as an end-resistance pile and vertical displacements of the pile was evaluated. Rezazadeh and Eslami [17] performed laboratory investigation on rock socketed piles and studied behavior of pile under compression load. Also calculated axial capacity and skin friction of piles. Walter *et al* [18] proposed model pile design only on shaft friction, with the goal of being economical design. However, the economical construction is not always financially sustainable. Research study suggested several solutions, such as socketed piles, to increase the performance of bored piles. Researchers have found the pile bearing problem is caused by surroundings and pile tip mud. Gavin and Lehane [19] carried out a number of field and laboratory studies on prototype pile, demonstrating that the pile base capacity can only be deployed, when the pile sinks enough to completely avoid the soft layer beneath the pile. In accordance with Zhang *et al* [20] the presence of mud below the pile and the drilled hole, may result in reduction in resistance, and higher settlements for drilled pile. Dai *et al* [21] and Maralapalle and Hegde [22] did identical prototype testing on cast-in -situ pile with debris.

In recent years, the rapid expansion of numerical techniques has created new opportunities in geotechnical modelling. A considerable number of these approaches are dedicated to dealing with large displacement problems [23–25]. This numerical study used the PLAXIS 3D software. It is a FEM application specifically designed to examine deflections in three dimensions of foundations [26, 27]. Boreholes are utilized to identify soil layers, and quadratic 10-node wedge components are used to replicate the soil's nonlinear behavior. The PLAXIS software provides 3D graphical representation of the computational results [28–30]. Additional improvements are made to the soil segment around the pile to improve accuracy further [31, 32]. To improve accuracy, the adjacent soil area is enhanced [33, 34]. The analysis is divided into three stages, including estimation of ground stresses in part I, modeling of pile placement in part II, and transfer of compression load to the pile top in part III. Within the finite element software, the load transfer occurs in increments of up to 50 iterations. Settlement and stress data are shown in tables and contour maps in the PLAXIS output program.

The load-displacement graphs provide maximum displacement measurements [35, 36].

This study encompasses a series of experimental investigations involving aluminum model piles in sandy soil conditions. These experiments are conducted under controlled conditions, both with and without the presence of a tip sponge. A constant load is applied to facilitate the comprehensive analysis of the load-settlement behavior exhibited by the piles. To enhance our understanding of the pile's response to axial loading, the experimental and numerical data are presented separately, allowing for a detailed examination of the pile's performance.

2. Experimental investigation

The planned experimental tests included instrumented pile testing, with the purpose of delivering additional information on skin friction mobilization in sand and load transfer procedures.

2.1 Test tank

Small scale studies are frequently employed to study pile behavior since field or prototype research is expensive. For example, Matsui *et al* [29] observed soil pressure working on horizontally driven pile with a diameter of 40 mm in a metal tank 600 mm long, 300 mm wide, and 300 mm deep. A research study conducted by Suleiman *et al* [30] in which they examined the behavior of a pile with a diameter of 102 mm that was inserted into a soil box with specific dimensions. The soil box had measurements of 1500 mm in length, 1500 mm in width, and 2250 mm in depth. One important aspect of the study was the ratio between the shorter dimension of the soil box and the diameter of the pile. This ratio ranged from 7.5 to 55, meaning that they considered various configurations where the soil box's shorter dimension was between 7.5 and 55 times the diameter of the pile. This wide range of ratios indicates that the researchers investigated a broad spectrum of soil-structure interaction conditions to assess how different geometries might affect the behavior of the pile. In technical terms, this research likely aimed to explore how different soil box sizes, relative to the pile size, influence the performance and behavior of the pile when subjected to various loads or conditions.

In this investigation, a testing tank formed of 6 mm thick mild steel plate with inside dimensions of 1 m × 1 m × 1 m (deep). The predicted proportion of the tank size to the pile size is 16.66. As a result, it is assumed that loaded pile response is unaffected by boundary condition. Although the tank size is thought to be enough, a friction reducing procedure was added along the side of the tank to even further removed border influences, grease was applied on the side wall of the tank.

2.2 Materials

In this investigation, sand was used as a backfill material in the test tank. Table 1 summarizes model ground properties of the sand utilized in this investigation. According to the IS: 2386 (Part I) [31], the sand was categorized as poorly graded sand (SP). Figure 1 depicts the grain size distribution result. All sand particles are filtered through a standard sieve, based on a sieve examination of the utilized sand, $D_{10} = 0.5$ mm, $D_{30} = 1$ mm, and $D_{60} = 1.70$ mm are determined. The cohesion and friction angle were measured using a series of direct shear experiments. as $c = 12$ kPa, and $\phi = 21^\circ$, respectively.

2.3 Model pile

In experimental studies, piles were simulated using aluminum, as shown in figure 2. The hollow aluminum Pipe was cut at regular interval to simulate required (Ls/D) ratio. The diameter of pile 60 mm with thickness of 6 mm were utilized in the lab test. Embedded lengths (Ls) of the pile ranged from 4D to 6D of the pile. Polyethylene sponge is composed of millions of microscopic gas compartments, each of which is enclosed by solid material. In this case, the sponge material is modeled as linear elastic. Linear elastic materials deform proportionally to the applied load within their elastic limit and return to their original shape once the load is removed. Poisson's Ratio (μ) is a measure of a material's deformation behavior under load. It relates to the lateral strain to the axial strain. A value of 0.3 indicates that the sponge material exhibits moderate deformation characteristics when subjected to loads. Young's Modulus (E) is a determine stiffness of material. A greater Young's Modulus indicates greater stiffness. In this case, the sponge material has a Young's Modulus of 3×104 kPa, indicating its stiffness level. Due to its great compressibility, sponge was utilized to classify the loose material at the tip of the pile. The sponge was trimmed to the pile size and pasted at

Table 1. Characteristics of the model ground.

| Sand characteristics | Value |
|-----------------------------------|-------|
| D_{10} (mm) | 0.5 |
| D_{30} (mm) | 1 |
| D_{60} (mm) | 1.7 |
| Average void ratio, e | 0.606 |
| Specific gravity, G | 2.60 |
| Maximum void ratio, e_{max} | 0.812 |
| Minimum void ratio, e_{min} | 0.497 |
| Coefficient of curvature, C_c | 1.17 |
| Coefficient of uniformity, C_u | 3.4 |
| Relative density, Dr (%) | 65 |
| Dry unit weight, γ_d (kPa) | 16.20 |
| Sand classification | SP |

the pile tip. Table 2 describes the sizes of the experimental pile utilized in the research. In the laboratory, the pile material was tested to determine its modulus of elasticity (69.32 GPa) and Poisson's ratio (0.312).

2.4 Instrumentation of piles

Strain gauges were attached to this hollow pile by cutting them at set increments. In this model pile, CN glue was used to secure the strain gauges. Figure 2 shows a model pile with gauges installed. The exterior of the pile was given knurling that was 0.5 mm \times 0.5 mm \times 0.5 mm deep so that it would look like the irregular surface in between the embedded substance and pile.

To enable practicality, internal strain gauges were affixed to the aluminum model pile. The model pile was segmented into multiple sections, with each section featuring a threaded connection to facilitate the assembly of individual pile units. Each segment had a height of 50 mm. To attach the strain gauges, CN adhesive was used to affix them to an aluminum pipe. To ensure their protection during testing, the strain gauges were covered with a water-proof substance. The wires from the strain gauges were carefully threaded through two pre-drilled holes positioned at opposite ends of the head of each pile. To guarantee water resistance, we applied a readily available waterproofing sealer named Crackseal to the strain gauge assembly. The configuration of strain gauges with 60 mm diameter pile is visually depicted in figure 3 for reference.

2.5 LVDT

Two LVDTs (Linear variable displacement transducers) were used to monitor displacement (settlement), and they were secured to the pile cap by means of a metal ring with flanges. This allows us to determine the typical displacement measured by the two LVDTs. For the purpose of calculating the axial force transmission and measuring the pile settling, LVDT was used. The smallest increment the LVDT can measure is 0.25 mm, and its maximum measuring range is 25 mm.

2.6 Load cell

To monitor the load transmitted to the pile, a load cell with a 20 kN capacity and a minimum count of 1 N is employed. The load cell is connected to a hydraulic system and is linked to a data recorder.

2.7 Data recorder

The instrumentation setup was utilized to gather data from the load cell, LVDTs, and strain gauges. The data recorder

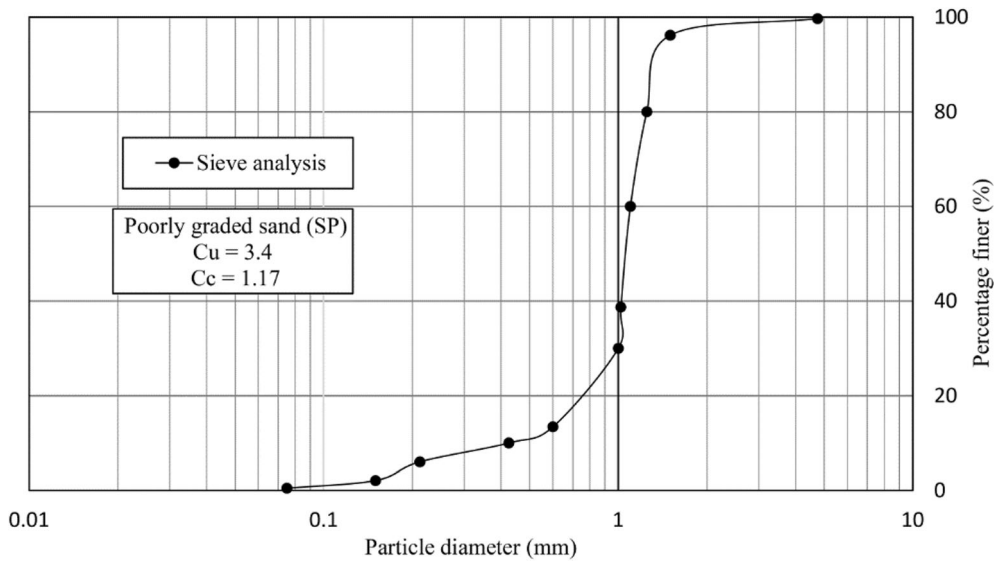


Figure 1. Curve of grain-size distribution.

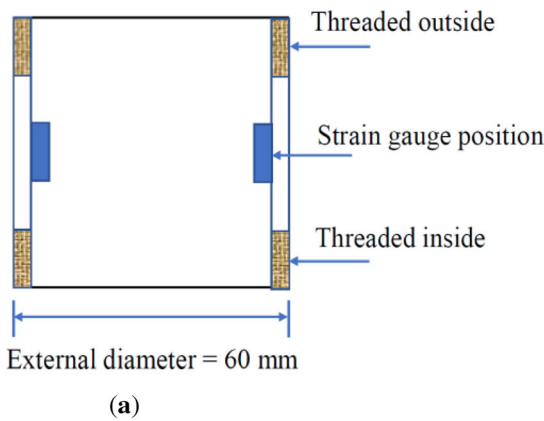


Figure 2. (a) The typical pile section and (b) Strain gauges Strain gauges are installed along the pile.

Table 2. The model pile’s characteristics.

| Model pile | Value |
|--|-----------|
| Length, L (mm) | 240, 360 |
| thickness, t (mm) | 6 |
| Outer diameter, D (mm) | 60 |
| Cross sectional area, A (mm ²) | 537.21 |
| Poisson’s ratio, μ | 0.312 |
| Moment of inertia, I (mm ⁴) | 218779.72 |
| Modulus of elasticity, E (GPa) | 69.32 |

effectively captures the pile’s axial load and strain, which is then used to determine the skin friction present within the embedded section.

2.8 Scaling of physical model

Small-scale modelling is effective solution in comparison to field study, allowing simulation observation of soil–structure interface. The experiments were conducted in a fairly rigid metal tank having 1 m × 1 m × 1 m depth. Phillips and Valsangkar [32] claimed in their laboratory examination that the rigid boundary has no effect when penetrating experiments are done at a length more than 5 d from the wall of the tank, and when the pile base is 10–12 d away from the tank’s bottom, till that there is no boundary influence. The tank dimensions were chosen based on these considerations to ensure that stress bulbs created surrounding the piles do not overlap with the tank sidewall and tank bottom. Ovesen [33] determined that the grain size impacts are negligible if (d/D₅₀) is between 25 and

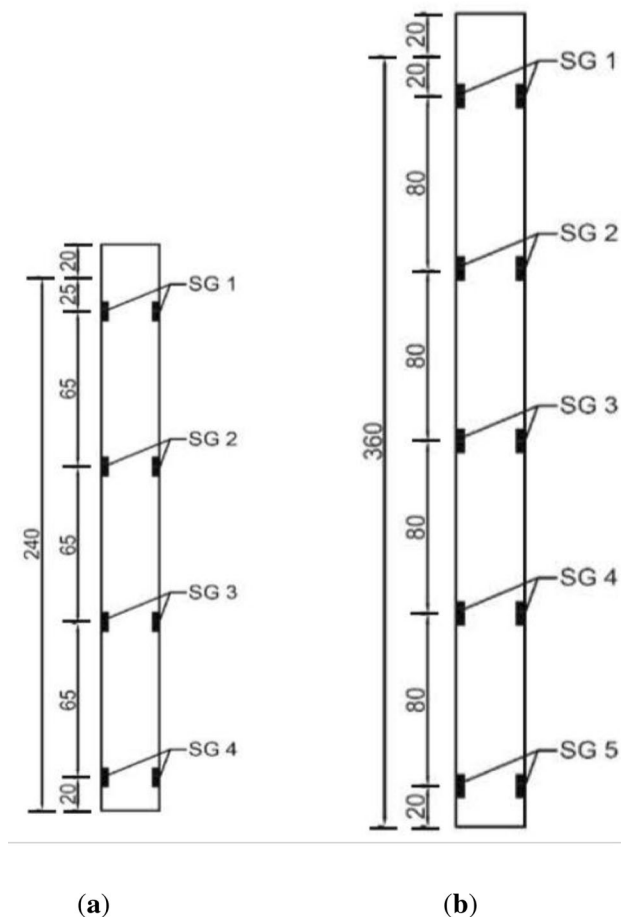


Figure 3. Strain gauge's location on piles. (a) = $L_s/D = 4$ and (b) = $L_s/D = 6$.

128 after performing a set of pull-out experiments on model anchors.

3. Experimental setup

Laboratory experiments were conducted within a loading frame. The laboratory test arrangement is depicted in figure 4. The compaction method of the sand was uniformed to obtain a constant density and remove any trapped air voids, following the guidelines outlined in the Indian Standard: 516 [34]. Each layer of the compaction process had a 50 mm thick and received 50 blows from a normal tamping rod. The tamping rod utilized in the experiments had a 16 mm diameter, a 600 mm length, and a bullet-shaped tip at the bottom. The rod's movements were uniformly dispersed throughout the tank's cross section to attain an average relative density of approximately 65% on average.

The experimental setup allowed for the incremental application of vertical load using a bolt connected a hydraulic jack. The hydraulic system was linked to the load

cell. Two LVDTs were placed upon flap supports attached to the pile's exactly against faces to record the movement of the pile top, as depicted in figure 4. In order to investigate pile load solely due to skin friction, complete elimination of end bearing was necessary. When there are layers of soft mud or clay just below the pile, this situation takes place in the foundation site. In the model pile, the end bearing effect was eliminated by affixing a 20 mm thick sponge to its bottom. The pile was then positioned in the tank and the surrounding sand material was compacted in layers.

Under the loading frame, the pile and assembly were put in place to convey the axial force. Digital data loggers were used to attach loading cells, strain gauge sensors, and LVDTs. Compressive loads were applied incrementally in steps of 10 N until failure occurred.

Utilizing a computerized displacement indicator, precise movement measurements were systematically gathered for every incremental load applied. Each load increment was sustained until the rate of pile displacement change reached a negligible level, typically achieved within a minute from the initiation of the load increment. Thorough records were maintained throughout the trials, encompassing applied loads, strain measurements, and settlements.

4. Modelling of geometry

For validating an experimental laboratory tests the numerical model was selected. Sand, sponge and pile modelling were carried out in software. The PLAXIS 3D software simulated model pile with and without sponge at the pile bottom. Cooke *et al* [35] studied a number of metal pile tests in the construction site, found that shear deformation beneath the soil, decrease to zero at a depth of $12D$ from the pile. To reduce the boundary effects for piles, Ni *et al* [36] recommended a $5D$ spacing between pile and side wall. The findings of pile resistant calculations for model having distance of $12D$ and $40D$ from bottom of the pile to tank bottom were found to differ by just 3%. As a result, a $12D$ model was used. Moreover, the effect of sand thickness was investigated, and the optimum number of 1.6 times the pile length is established. The surface sand was set as free while the sand bottom was set as fixed as the boundary condition. Bore log was created as per the required depth and sand simulation were done by Mohr-column model. Piles were modeled as linearly elastic material. Despite the fact that the model pile was hollow cylinder with plate at the top and at the end of pile, they were created using a mix of beam and solid elements. Length of the aluminum piles were 240 mm and 360 mm. Diameter of the piles was 60 mm. For $4D$ and $6D$ depths, the model piles were inserted in the layer of sand. In Table 3, the numerical model's inputs are listed in detail. Also, figure 5 displays the finite element model of sand,

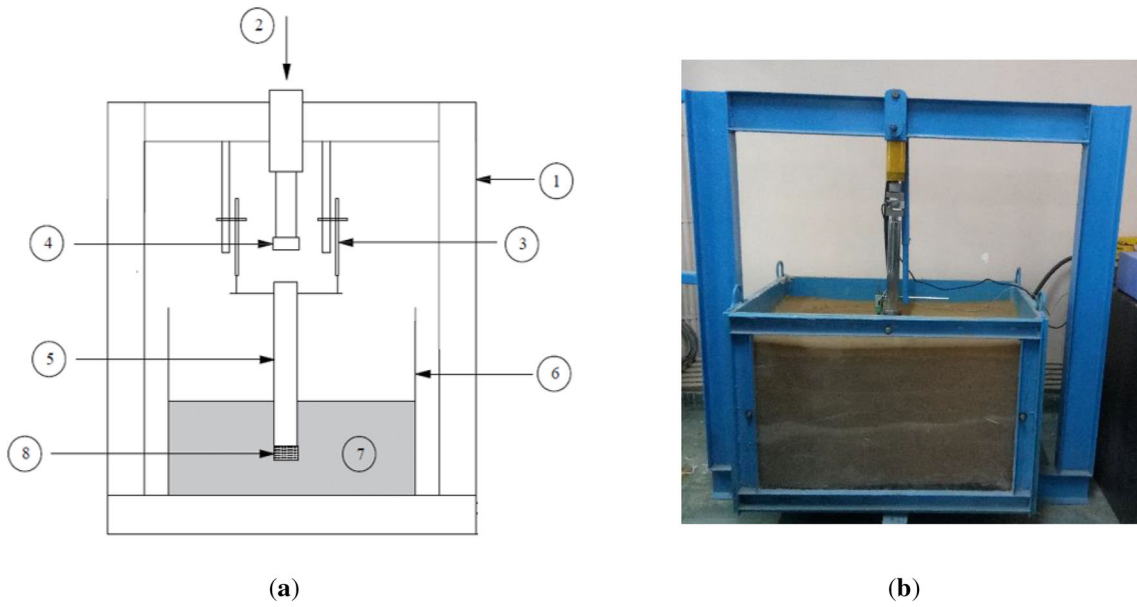


Figure 4. Set-up for the experiment (a) experimental Illustration (1= Loading structure, 2= Load cell, 3= LVDT, 4= hydraulic system, 5= model pile, 6 = tank, 7 = sand, 8 = Sponge) and (b) Pile load test set-up.

Table 3. Different element utilized in FEM modeling.

| Element | Aluminum pile | Sand | Sponge |
|--|------------------|------------------|-----------------|
| Model | Linear elastic | Mohr-column | Linear elastic |
| Unit weight, γ (kN/m ³) | 27 | 17.7 | 1.3 |
| Cohesion, C (kPa) | – | 5 | – |
| Friction angle, ϕ (degree) | – | 32 | – |
| Poisson's ratio μ | 0.30 | 0.35 | 0.3 |
| Young's modulus, E (kPa) | 69×10^6 | 20×10^3 | 3×10^4 |

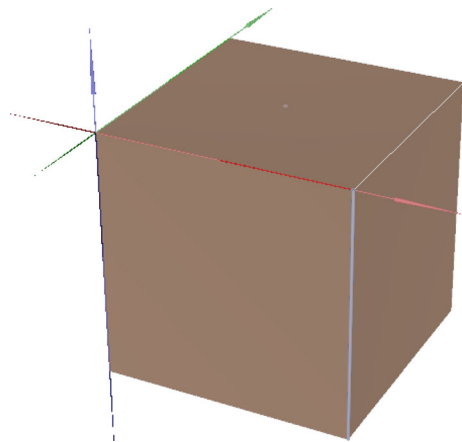


Figure 5. The FEM of the sand layer.

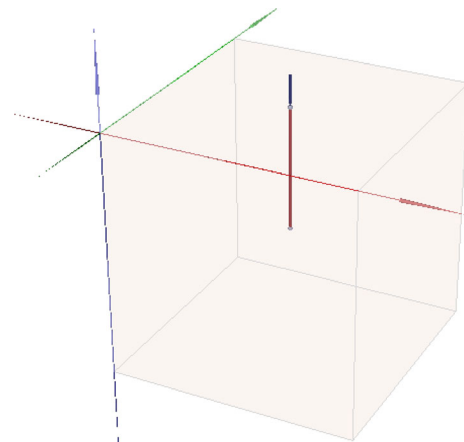


Figure 6. The FE model of the applied load and pile.

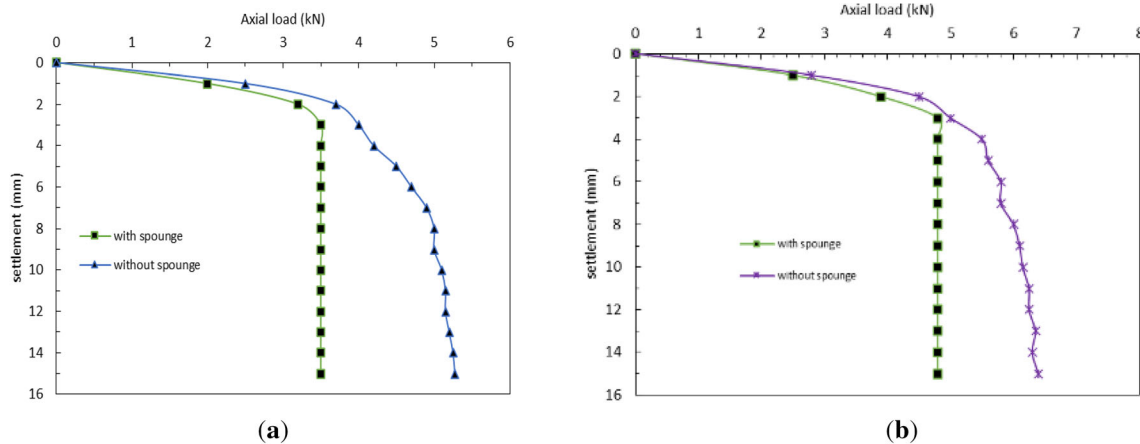


Figure 7. Illustration of the pile's load-settlement curve (a) $Ls/D = 4$ and (b) $Ls/D = 6$.

while figure 6 showcases the finite element model of the pile load.

4.1 Mesh and fineness effect

Following the completion of the geometry, the next step involved generating a finite element mesh. Mesh generation is the process of dividing the model, consisting of sand and structural elements, into volume elements to facilitate calculations. The size of the mesh elements has an impact on both the computation time and the accuracy of the results. By reducing the element size, the computation time increases while the accuracy of the results improves. In this study, a fine mesh size was employed for the modeling to achieve more accurate results.

4.2 Staged construction

Staged construction is the final step in the calculation. Different stages of the construction were specified in this step, similar to a real-life model, including initial condition, pile formation, and structural load application. All subsurface volumes were initiated during this phase, while all structural members and load were inactivated. The next stage was the generation of pile phase. In this phase pile and load were activated.

5. Experimental and numerical modelling results

The load-displacement curve for pile with and without a sponge at the base of the pile is depicted in figure 7. Pile's load-settlement curve initially displays a straight-line trend initially, followed by a nonlinear trend at a later stage. When loads are applied to a pile using a sponge, after the provided force surpassed the frictional resistance, the pile

may settle rapidly. The mean readings from the LVDTs were recorded to calculate the vertical settlement. An analysis of the load-settlement patterns for various Ls/D ratios is shown in figure 7. The observed loads were 3.5 kN and 5.3 kN, resulting in corresponding settlements of 15 mm (as depicts in figure 7a). Similarly, figure 7b shows the observed loads of 4.8 kN and 6.4 kN, with corresponding settlements of 15 mm. It was noticed that a higher Ls/D ratio caused the axial pile capacity to rise.

The strains measured from the skin resistance values acting on the pile's sides were computed using strain gauge measurements. Equation (1) is used to calculate the skin resistance force (Q) within the pile.

$$Q = \varepsilon EA \quad (1)$$

The measured strain (ε) is used in Equation (1), where E represents the model pile's modulus of elasticity, and A denotes the pile's area of cross-section. The load distribution characteristics were investigated based on the values of calculated strain. Skin resistance forces were determined at different levels along the pile using Equation (1). Figure 8a, b provide axial load data for piles with a slenderness ratio (Ls/D) of 4, comparing those with and without a sponge material. In figure 8a, axial load was applied across pile lengths (25 mm, 90 mm, 155 mm, and 220 mm) for piles with a sponge, showing that the sponge reduces axial load capacity, with decreasing capacity as the pile length increases. Figure 8b displays different axial load for piles without a sponge, demonstrating higher axial load capacities compared to those with a sponge, particularly for longer piles. Furthermore, non-linear relationships between axial load and pile length are observed, especially at higher load levels. Figure 9a, b introduce piles with a Ls/D ratio of 6, reinforcing the trends seen in figure 8a, b, with the sponge material reducing load capacities. when the pile's top is subjected to axial stresses. These data demonstrate that when the Ls/D ratio rise, the piles' load-bearing

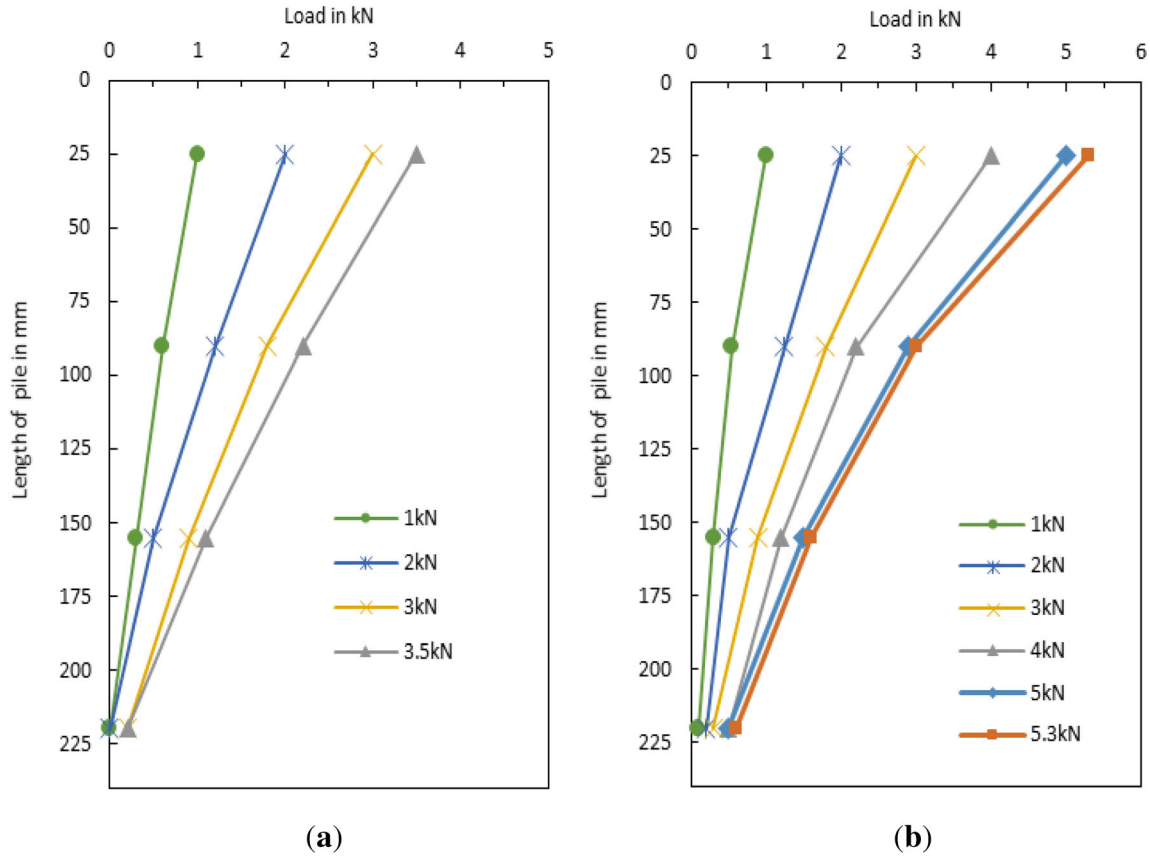


Figure 8. The pile’s axial load, $L_s/D = 4$ (a) with sponge and (b) without sponge.

capacity rise as well. The piles’ tops showed the highest skin frictional load which steadily dropped throughout the depth of the piles, reaching a low at the base of the pile. Considering the vertical equilibrium of the pile, the transmitted load was discovered to have an inaccuracy between $- 5\%$ and $+ 7\%$, and to be almost comparable to the skin frictional forces.

5.1 Unit skin friction estimation

The skin resistance forces were calculated at various strain gauge positions to evaluation the unit skin resistance. The unit skin resistance (f) generated within those two strain gauge levels is obtained by dividing the variations within the skin resisting forces by the side surface area of the pile across successive strain gauges.

Equation (2) can be used to calculate the unit skin friction ‘ f ’ for a specific section of the pile length.

$$f = \frac{\Delta Q}{\pi DL} \tag{2}$$

Equation (2) utilizes ΔQ , which represents the variation in the axial load measured by the pile’s subsequent strain gauges. D represents the diameter of the pile, and L

corresponds to the distance in between the following strain gauges. The Unit skin resistance varies over the depth of piles with L_s/D ratios of 4 and 6 is depicted in figures 10 and 11, respectively. Generally, mobilized skin resistance tends to rise as the axial force rises until it reaches failure loads. The vertical loads calculated at the strain gauge positions are used to compute the mobilized skin friction. Figure 10 illustrates that for piles with a L_s/D ratio of 4, the maximum skin friction values were 156 kPa and 187 kPa for piles with and without a sponge, respectively. Similarly, for piles with an L_s/D ratio of 6, the maximum skin friction values were 128 kPa and 210 kPa for piles with and without a sponge, respectively (as shown in figure 11). It is reported that the maximum development of skin resistance occurs at the top of the pile, and it reduces to zero for piles without a sponge. Piles with a sponge exhibit a smaller amount of maintained skin friction.

Similar findings were reported in the studies conducted by Dai *et al* [1] and Unsever *et al* [23] through finite element analysis. It was observed that the skin resistance at the pile base declines when the end bearing resistance becomes significant, increasing pile settlement as a result of sponge compression, as demonstrated in figures 10 and 11. This observation aligns with the findings of Meijuan Xu *et al* [26] and Dong [37].

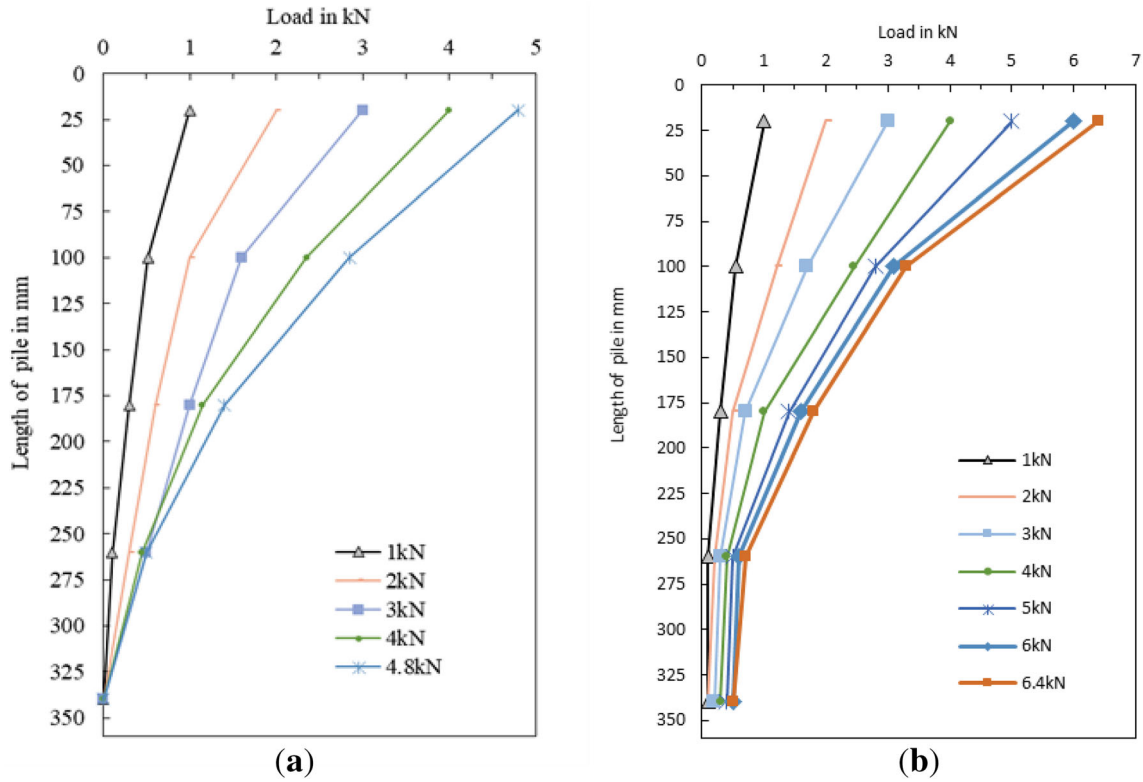


Figure 9. The pile’s axial load, $L_s/D = 6$ (a) with sponge and (b) without sponge.

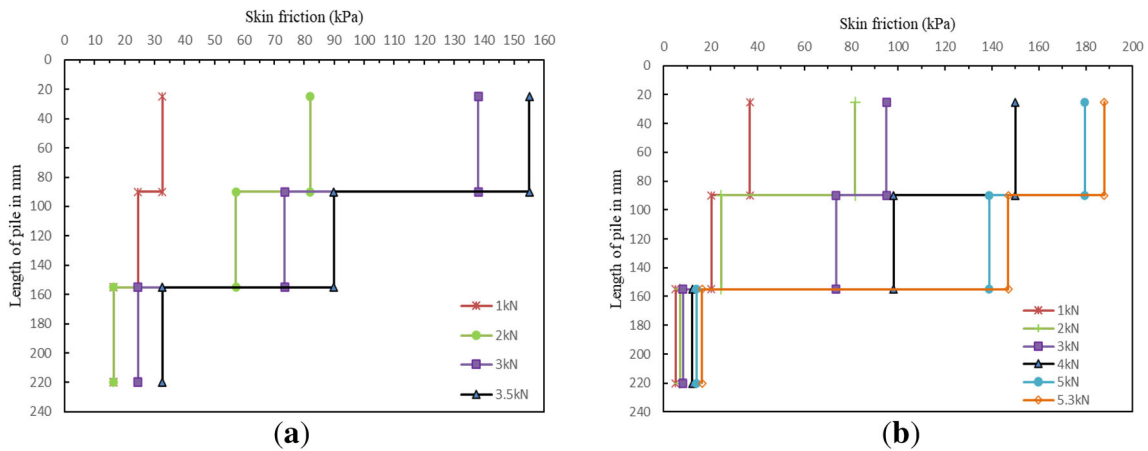


Figure 10. Skin friction for pile, $L_s/D = 4$. (a) with sponge and (b) without sponge.

5.2 Output of modelling

The analysis’s output stage offers significant insights into the stress distribution within the model, pinpointing critical stress regions. Furthermore, it presents key information such as vertical displacement, maximum stress values, and post-loading contours. Notably, figure 12 illustrates the vertical displacement following the application of the load.

A comparison between the load-settlement curves observed in laboratory tests and simulation studies is presented in figure 13. It is evident that the simulated measurements adequately describe the performance of piles with and without a sponge. However, it should be noted that the numerical settlement values for both piles are slightly lower than the experimentally measured values for a given load.

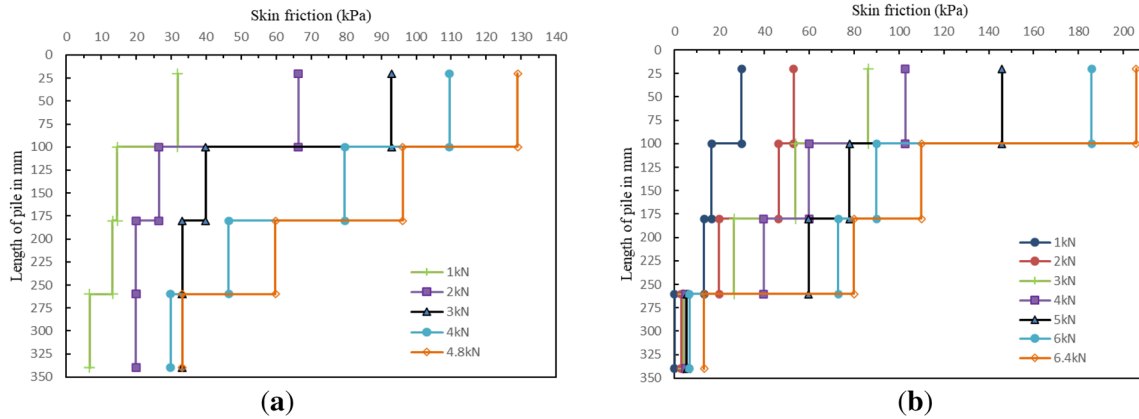


Figure 11. Skin friction for pile, $L_s/D = 6$. (a) with sponge and (b) without sponge.

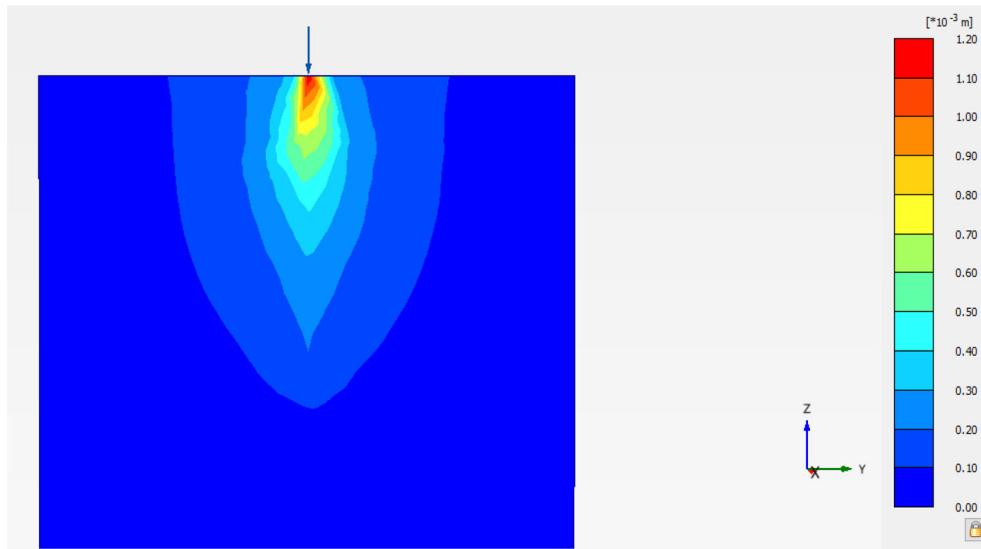


Figure 12. FE model for total settlement.

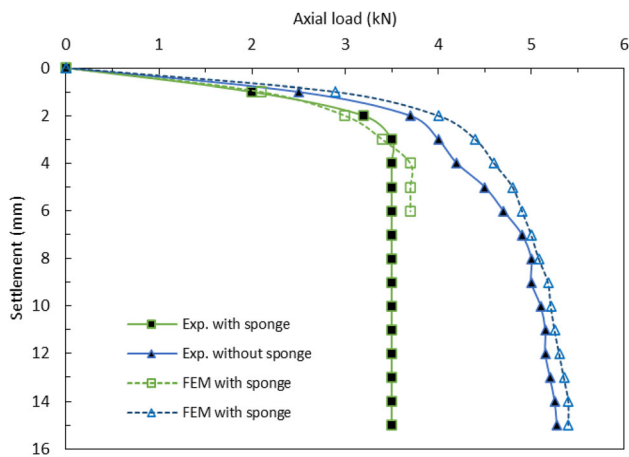


Figure 13. Comparison of load-settlement curves of experimental and FEM modeling for pile (4D) depth.

Figure 14 illustrates the load distribution in the pile, with corresponding numerical values extracted from the computations. The axial load in the pile follows a consistent pattern under various applied loads, with a higher load concentration at the pile top and decreasing towards the depth. The pile capacity for the pile with a sponge is predominantly produced by skin friction, as seen by the comparatively low applied load communicated to the pile base. As the load increases, the compressed area of the sponge beneath the pile compresses, and the contribution from the pile base reaction becomes more significant. The skin resistance along the depth of the pile, with and without a sponge, was determined based on figure 14. Generally, as the loading increases, higher skin resistance is acting at the pile top compared to the pile bottom. Once the pile base reaction begins to occur, Skin resistance drops near the base of the pile. The compression of the sponge leads to

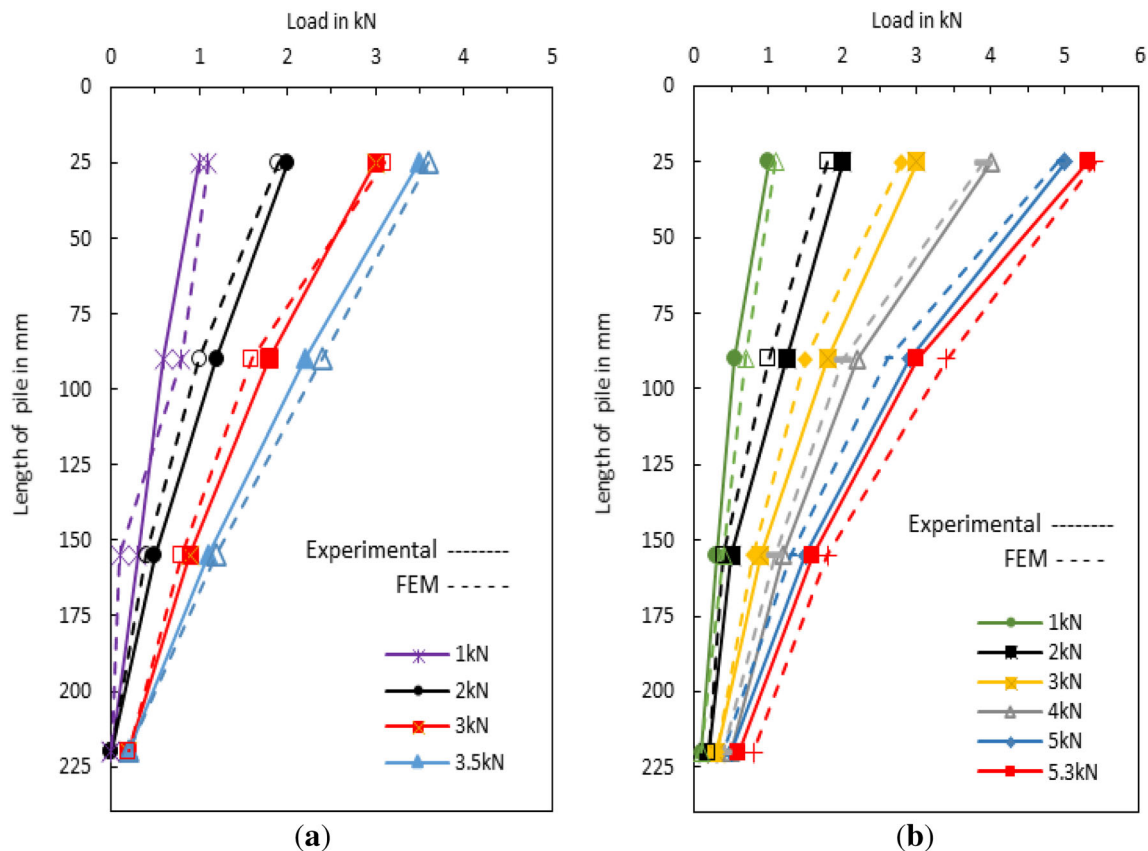


Figure 14. Comparison of axial forces from experimental and numerical modeling: (a) Pile with sponge and (b) Pile without sponge.

significant pile movement and increased sand-pile slippage. Consequently, the sponge mobilizes higher skin friction for the pile. This finding is in accordance with Dong's [37] the observations that a soft layer beneath the base of the pile can facilitate the development of skin resistance there.

6. Conclusion

The objectives of this ongoing investigation is to examine the behavioral properties of piles when they are embedded in a sand medium. The research specifically focuses on shedding light on the skin friction behavior of piles in sandy substrates, both with and without the inclusion of a sponge material. In order to comprehend the frictional mechanisms governing pile foundations, a number of axial load tests were systematically conducted on a single pile model, conducted within a dry sand environment.

Also, tests were modelled using FEM to develop a better understanding of the systems and to investigate a viable design technique. The numerical simulations for the several trials were done with a specific set of sand characteristics for the modeling ground. The numerical computation successfully simulated the trends of the laboratory findings. As per the practical significance of the research is concern, this

knowledge is crucial for civil and geotechnical engineers who design foundations for structures. The practical significance of this research lies in its potential to improve the design and construction of foundations, especially in dry sand conditions. Engineers can use the findings to make informed decisions about pile materials, dimensions, optimize pile configurations for specific projects, cost-effectiveness, and installation techniques, ultimately leading to safer and more stable structures.

The following are the key findings drawn from the investigations undertaken in this study.

1. Piles with a sponge exhibit reduced bearing capacity compared to piles without a sponge. This suggests that the presence of a sponge at the base of the pile affects its ability to resist vertical loads. The sponge material's compressibility or deformability, which results in reduced support and load-bearing capacities, are likely to be responsible for the decreased bearing capacity.
2. The top of the pile encounters a higher rate of skin resistance when exposed to compressive axial loads. This indicates that the upper portion of the pile has a more noticeable frictional interaction with the surrounding soil. However, the rate of skin resistance steadily reduces as we proceed down the length of the pile. This

change in skin resistance over the length of the pile could have an impact on its total capacity for supporting loads and settlement behaviours.

3. Several finite element (FE) models were utilized to study the behaviour of piles with and without sponges. They were able to determine load settlement curves using these numerical models, which offer significant insight about how the piles respond to various loads and soil characteristics. To validate the models' reliability and accuracy, numerical simulations and experimental data were compared.
4. There is a significant correlation between the load-displacement curves from the numerical simulation and the laboratory investigation. This suggests that the numerical models correctly represented pile's behaviour under various loading circumstances. Less than $\pm 5\%$ of displacement difference was detected between experimental and numerical findings, demonstrating acceptable agreement between the two methods.

In summary, the pile bearing capacity is impacted by the sponge's presence at the base, and the load settlement behaviour is influenced by the sponge's compressibility. The research demonstrated the validity of finite element models in predicting pile behaviour and emphasized the importance of considering such factors when designing and analysing pile foundations in practical engineering applications.

References

- [1] Dai G, Salgado R, Gong W and Zhu M 2017 The effect of sidewall roughness on the shaft resistance of rock-socketed piles. *Acta Geotech.* 12(2): 429–440
- [2] Basu P, Loukidis D and Prezzi M 2011 Analysis of shaft resistance of jacked piles in sands. *Int J Numer. Anal. Meth. Geomech.* 35(15): 1605–1635
- [3] Nasr A M 2013 Experimental and theoretical studies of laterally loaded finned piles in sand. *Can. Geotech. J.* 51(4): 381–393
- [4] Beredugo Y O 1966 An experimental study of the load distribution in pile groups in sand. *Can. Geotech. J.* 3(3): 145–166
- [5] Drbe osama and Naggat M H, 2014 Axial monotonic and cyclic compression behaviour of hollow-bar micropiles. *Geotech. Test. J.* 52(4): 426–441
- [6] Paik K, Salgado R, Lee J and Kim B 2003 Behavior of open- and closed-ended piles driven into sands. *J. Geotech. Geoenviron. Eng.* 129(4): 296–306
- [7] Yang J, Tham L, Lee P, Chan S and Yu F 2006 Behaviour of jacked and driven piles in sandy soil. *Géotechnique.* 56(4): 245–259
- [8] Zhao C F, Lu J, Sun Q C, Zhu T and Li S F 2009 Experimental study of load transmission property of large-diameter bored cast-insitu deep and long pile in different soil layers. *Chin. J. Rock Mech. Eng.* 28(5): 1020–1026
- [9] Cao X D, Wong I H and Chang M-F 2004 Behavior of model rafts resting on pile-reinforced sand. *J. Geotech. Geoenviron. Eng.* 130(2): 129–138
- [10] Lam S Y, Ng C W W, Leung C F and Chan S H 2009 Centrifuge and numerical modeling of axial load effects on piles in consolidating ground. *Can. Geotech. J.* 46(1): 10–24
- [11] Onuselogu P and Yin Z 1998 Pile behaviour in sand through experiments. *Chin. J. Geotech. Eng.* 20(3): 85–99
- [12] Matsumoto T, Fukumura K, Kitiyodom P, Oki A and Horikoshi K 2004 Experimental and analytical study on behaviour of model piled rafts in sand subjected to horizontal and moment loading. *Int. J. Phys. Model Geotech.* 4(3): 1–19
- [13] Al-Mhaidib A I 2006 Experimental investigation of the behavior of pile groups in sand under different loading rates. *Geotech. Geol. Eng.* 24(4): 889–902
- [14] Han Z, Vanapalli S K and Kutlu Z N 2016 Modelling the behavior of a friction pile in compacted glacial. *Int. J. Geomech.* 16(6): D4016009
- [15] Maralapalle V and Hegde R 2022 An experimental study on the socketed pile in soft rock. *Eng. Technol. Appl. Sci. Res.* 12(6): 9665–9669
- [16] Zhao B, Wang X, Yang M, Liu D, Liu D and Sun S 2020 Experimental study on static load of large-diameter piles in non-uniform gravel soil. *Adv. Civ. Eng.* 2020: 1–15
- [17] Rezazadeh S and Eslami A 2017 Empirical methods for determining shaft bearing capacity of semi-deep foundations socketed in rocks. *Int. J. Rock Mech. Geotech. Eng.* 9(6): 1140–1151
- [18] Walter D, Burwash W and Montgomery R 1997 Design of large-diameter drilled shafts for the Northumberland Strait bridge project. *Can Geotech. J.* 34(4): 580–587
- [19] Gavin K and Lehane B 2007 Base load–displacement response of piles in sand. *Can. Geotech. J.* 44(9): 1053–1063
- [20] Zhang Z-M, Yu J, Zhang G-X and Zhou X-M 2009 Test study on the characteristics of mudcakes and in situ soils around bored piles. *Can. Geotech. J.* 46(3): 241–255
- [21] Dai G, Gong W, Zhao X and Zhou X 2011 Static testing of pile-base post-grouting piles of the suramadu bridge. *Geotech. Test. J.* 34(1): 34–49
- [22] Maralapalle V and Hegde R 2022 Model studies on effect of pseudo-rock-socket strength on resistance of friction-only piles. *Eng. Sci. Technol. Int. J.* 34: 101089
- [23] Unsever Y S, Smoto T and Ozkan M Y 2015 Numerical analysis load tests on model foundations in dry sand. *Comput. Geotech.* 63: 255–266
- [24] Gutiérrez-Ch J G, Melentjevic S, Senent S and Jimenez R 2020 Distinct element method simulations of rock-socketed piles: estimation of side shear resistance considering socket roughness. *J. Geotech. Geoenviron. Eng.* 146(12): 04020133
- [25] Zhang C-s, Wang Y-h, Xiao H-b and Fan Z-h 2009 Theoretical analysis and numerical simulation of load-settlement relationship of single pile. In: *GeoHuman International Conference, Changsha, Hunan, China*, pp. 126–132
- [26] Meijuan X, Ni P, Mei G and Zhao Y 2018 Load-settlement behaviour of bored piles with loose sediments at the pile tip: experimental, numerical and analytical study. *Comput. Geotech.* 102: 92–101
- [27] Franke E, Lutz B and El-Mossallamy Y 1994 Measurements and numerical modelling of high-rise building foundations on Frankfurt clay. In: *Proceedings of a conference on*

- vertical and horizontal deformations of foundations and embankments*. 40: 1325–1336
- [28] Reul O 2004 Numerical study of the bearing behaviour of piled rafts. *Int. J. Geomech.* 4(2): 59–68
- [29] Matsui T, Hong W P and Ito T 1982 Earth pressures on piles in a row due to lateral soil movements. *Soils Found.* 22(2): 71–81
- [30] Suleiman M T, Ni L and Raich A 2014 Development of pervious concrete pile ground-improvement alternative and behavior under vertical loading. *J. Geotech. Geoenviron. Eng.* 140(7): 04014035
- [31] Indian Standard: 2386 (Part I) 1963 *Method for test for aggregates for concrete*
- [32] Phillips R and Valsangkar A J 1987 *An experimental investigation of factors affecting penetration resistance in granular soils in centrifuge modeling*. Cambridge University Engineering Department, Cambridge, UK. Technical Report
- [33] Ovesen N K 1981 Centrifuge tests of uplift capacity of anchors. In: *Proc., 10th Int. Conf. Soil Mechanics and Foundation Engineering*, Sweden. 717–722
- [34] Indian Standard: 516 2006 *Method of tests for strength of concrete*
- [35] Cooke R W, Bryden Smith D W, Gooch M N and Sillet D F 1981 Some observations of the foundation loading and settlement of a multi-storey building on a piled raft foundation in London Clay. *Proc. Inst. Civ. Eng.* 107(1): 433–460
- [36] Ni P, Qin X and Yi Y 2018 Numerical study of earth pressures on rigid pipes with tire-derived aggregate inclusions. *Geosynth. Int.* 25(5): 494–506
- [37] Dong J 2009 Enhanced and weakened effect of skin friction of cast-in-situ piles. *Chin. J. Geotech. Eng.* 31(5): 658–662